JOURNAL OF GEOPHYSICAL RESEARCH, VOL. 113, C12024, doi:10.1029/2008JC005075, 2008



# Observations of swell influence on ocean surface roughness

Paul A. Hwang[1]

Received 8 August 2008; revised 29 September 2008; accepted 21 October 2008; published 27 December 2008.

[1] Field measurements of the ocean surface wave spectrum focusing on the slope-contributing components are used to construct a spectral model of the ocean surface roughness. The spectral parameterization is established with the observed empirical power law relation between the dimensionless wave spectral density and wind speed. The power law parameters (proportionality coefficient and exponent) are shown to be modified by swell. Discussions are presented on the swell effects of spectral properties, including their wind speed dependence and swell modification of roughness components characterizing Bragg resonance and surface tilting in radar application. Several notable results include the following: (1) With increasing swell intensity, the spectral density increases in the long-wave portion and decreases in the short-wave portion of the intermediate-scale waves. (2) There is a nodal point with respect to swell impact in the wave number dependence of the coefficient and exponent of the spectral parameterization function in the vicinity of wave number near 3 rad/m, suggesting that waves about a couple of meters long are insensitive to swell influence. (3) Spectral density in the decimeter length scale becomes less sensitive to wind speed variation as swell intensity increases. (4) Increasing swell influence shifts wave breaking toward shorter and broader scales.

**Citation:** Hwang, P. A. (2008), Observations of swell influence on ocean surface roughness, *J. Geophys. Res.*, *113*, C12024, doi:10.1029/2008JC005075.

## 1. Introduction

[2] Surface roughness plays an important role in remote sensing of the environment. In active or passive mode, the signal characteristics scattered or emitted to the sensor are critically dependent on the roughness condition. In ocean remote sensing, the surface roughness is primarily contributed by surface waves. The length scale of a surface wave is important in quantifying its contribution to the surface roughness and the resulting remotely sensed signal. For example, for a scatterometer that typically operates at a moderate incident angle between about 20 and 60°, surface roughness components with wavelengths close to the electromagnetic (EM) wavelength contribute to Bragg resonance; those shorter than the Bragg wavelength cause signal diffusion and those longer tilt the scattering elements and change the effective (local) incident angle. Accurate interpretation of the remote sensing signal relies on a clear understanding of the response of these roughness-contributing surface waves to various geophysical parameters such as wind velocity, background waves and currents.

[3] The ocean surface roughness is traditionally quantified by the mean square slope (mss). For a sinusoidal surface wave train, the mss is proportional to the square of the product of wave amplitude and wave number. The short-scale waves (with large wave number $k$), therefore, make the most contribution if the ocean surface spectrum is broad band approaching a white noise. Our understanding of the ocean surface wave spectrum is mainly derived from waves of maximum amplitude near the "elevation" spectral peak. Several notable spectral models have been established with measurements of wind generated waves in open waters: that of *Pierson and Moskowitz* [1964] for fully developed condition, and *JONSWAP* [*Hasselmann et al.*, 1973] and that of *Donelan et al.* [1985] for fetch limited condition. Because of their long wavelengths (small $k$), the mss contributed by the large waves near the elevation spectral peak region is typically small as can be easily verified from integrating the wave slope spectrum [e.g., *Hwang and Wang*, 2001, section 3]. Conducting measurements of short-scale waves in the ocean is a very difficult task. Spectral models extending to short-scale waves generally rely on laboratory measurements and theoretical reasoning. Extensive discussions of several published models, including those of *Bjerkaas and Riedel* [1979], *Donelan and Pierson* [1987], *Apel* [1994], *Elfouhaily et al.* [1997] and *Plant* [2002], have been presented in the last two references and will not be repeated here. It is well known that a direct transfer of laboratory results to ocean condition can cause serious problem in the quantification of the spectral properties of wind generated waves because of the difficulty in satisfying simultaneously the gravity (Froude number), capillary (Weber number) and viscosity (Reynolds number) similarity conditions in laboratory experiments [*Hwang*, 1997, section 2b]. The Froude number similarity is important in ensuring correct simulation of surface gravity waves, the

[1]Remote Sensing Division, Naval Research Laboratory, Washington, DC, USA.


0148-0227/08/2008JC005075$09.00

Weber number similarity is important in ensuring correct simulation of surface capillary waves, and the Reynolds number similarity is important in ensuring correct simulation of wind forcing and air-sea momentum transfer. In order to properly apply the wind generated water surface roughness data derived in the laboratory to the ocean condition, the fluid dynamics similarity and scaling issues have to be unraveled. To my knowledge, this has not been reported in open literature. On the other hand, theoretical models tend to be overly simplified in comparison to the natural conditions because of the complex dynamics of short-scale waves and many of the parameters in the theoretical framework require quantification with experimental data that are not available for the ocean environment.

[4] Rather than extending the wave spectrum from the long-wave region that is important to the surface wave height, *Hwang* [2005] reports a wave spectral model focusing on the region of dominant wave slope contribution using field measurements of ocean surface waves with wavelengths ranging from 6 m down to about 2 cm ($1 \leq k \leq 300$ rad/m, referred to as intermediate-scale waves, ISW, from here on). For such short waves, treatment of the Doppler frequency shift in the measurement is critical [e.g., *Hughes*, 1976; *West et al.*, 1990; *Hwang*, 2006]. The Doppler frequency shift problem is alleviated through Lagrangian measurement with fast response wave gauges carried on an open structure set in free drift. The application of linear dispersion relation for converting the frequency spectrum to the wave number domain is much more accurate in Lagrangian measurements [*Hwang and Wang*, 2004a, Figure 1]. The filtered mss integrated from the spectral model are found to be in good agreement with those derived from sun glitter measurements of *Cox and Munk* [1954] in clean and slick waters as well as Ku band (13.6 GHz, cutoff surface wave number about 63 rad/m) radar measurements reported by *Jackson et al.* [1992] (including measurements by *Jones et al.* [1977] and *Wentz* [1977]). Further comparison with radar measurements at Ka band (36 GHz, cutoff surface wave number 162 rad/m) [*Walsh et al.*, 1998; *Vandemark et al.*, 2004], C band (5.35 GHz, cutoff surface wave number 24 rad/m) [*Hauser et al.*, 2008] and low wave number mean square slope obtained with an airborne laser altimeter array [*Vandemark et al.*, 2004] is also reasonable (section 4).

[5] One of the prominent features revealed in the ISW spectral analysis is the swell effect. Earlier observations, mostly from laboratory experiments [e.g., *Plant and Wright*, 1977; *Donelan*, 1987], suggest that the presence of longer waves (mechanically generated "swell" in the laboratory experiments) suppresses the growth of short waves that would have grown prominently in the absence of the longer mechanical waves. Interpretations of this observation vary. A straightforward explanation emerges when considering the length scale of the mechanical waves generated in the laboratory facilities. The short mechanical wavelengths in the laboratory are well within the active wind generation frequency band. Their preexistence simply makes the growth of that particular frequency much more expedient, at a cost to the growth of other frequency components. In other words, the mechanical waves in those experiments are not swell, they are subjected to local wind forcing. *Hwang and Shemdin* [1988] present an analysis of their field data of ocean surface mean square slope combined with those collected by *Cox and Munk* [1954] and *Tang and Shemdin* [1983]. The result shows that the swell effect on surface roughness is not monotonic with respect to swell intensity. At low and moderated swell influence, either expressed by the wave age or long-wave steepness, the ocean surface roughness is enhanced. When the swell influence exceeds a certain level, the surface roughness is reduced [*Hwang and Shemdin*, 1988, Figures 9 and 10]. The swell effect, however, is complicated by the air-sea stability condition. If the stability effect is removed first, the swell effect becomes more difficult to discern and both enhancement and suppression of roughness coexist in a similar parameter range of swell influence [*Hwang and Shemdin*, 1988, Figures 15 and 16]. *Hwang and Wang* [2004a] divide their collection of the wave number spectra (in neutral stability condition) into two broad categories based on the ratio between the spectral densities in the low- and high-frequency ranges. Those results form the basis of *Hwang*'s [2005] spectral model development. In mixed seas, swell modifies the spectrum of intermediate-scale waves in a somewhat complex way. For waves shorter than about 1 m, spectral enhancement occurs at lower wind speeds but suppression at higher wind speeds. For longer ISW, the effect of swell is opposite to that for the shorter waves. The magnitude of the spectral fluctuations deviating from the reference condition (least swell influenced) is usually within about 20 percent for most ISW components in the data analyzed. The critical wind speed separating these two opposite trends is somewhat higher than 6 m/s. As will be seen in the next section, the wave conditions in the ISW spectral data set are relatively mild, with significant wave height mostly less than 1 m. It may be questioned whether the result are representative of open ocean conditions, of which typical wave heights are rarely less than 1 m. Remote sensing techniques are much more robust for operation in high sea states. Recently, *Hwang et al.* [2008b] report low grazing angle X band radar backscatter measurements from an ocean tower (radar wavelength 3 cm). The wave height in the data set ranges from 1.2 to 2.7 m. They also notice that in comparison with wind sea condition, the backscatter return is reduced when moderate swell is present. The result is suggestive of swell suppression of the spectral density in the centimetric wave range, which is consistent with the ISW spectral analysis described by *Hwang* [2005].

[6] Here, more refined division of the swell parameter is performed to the data set reported by *Hwang and Wang* [2004a]. The incremental variation of the ISW spectral properties as a result of increased swell effect can be more clearly evaluated. In the following, section 2 describes the analysis procedure and the spectral data collection. Section 3 presents the swell effects on the surface roughness spectrum as revealed in the properties of the spectral parameterization coefficients. Section 4 shows the computed roughness spectrum for a range of wind speed and swell condition. The mss integrated to the cutoff wave numbers according to different radar frequencies are compared with mss derived from radar measurements at Ka [*Walsh et al.*, 1998; *Vandemark et al.*, 2004], Ku [*Jones et al.*, 1977; *Wentz*, 1977; *Jackson et al.*, 1992] and C bands [*Hauser et al.*, 2008], as well as the sun glitter data in clean and slick waters [*Cox and Munk*, 1954] and long-wave mss obtained

by an airborne laser altimeter array [*Vandemark et al.*, 2004]. Section 5 presents discussions on the swell index, some issues on the data processing of the spectral components in the low wave number range of ISW and the limitation of the wind, wave and geophysical conditions in the data set, and section 6 is a summary.

## 2. Analysis Procedure and Data Description

### 2.1. Analysis Method

[7] The wave action conservation equation is frequently used to study the dynamics of ocean surface waves. In directionally integrated (omnidirectional) form, it can be written as

$$\frac{dN(k)}{dt} = S_{nl} + S_{in} + S_{ds}, \tag{1}$$

where $N(k)$ is the wave action, which is related to the surface elevation spectrum by $N(k) = g\chi(k)/\omega$, $\chi(k)$ the omnidirectional wave spectrum, that is, $\int \chi(\boldsymbol{k}) k d\theta$, $g$ the gravitational acceleration, $\omega$ the intrinsic frequency and $\boldsymbol{k}$ the wave number vector with modulus $k$. The three terms on the right hand side of (1) are the source functions of nonlinear wave-wave interaction, wind input and breaking dissipation. Theoretical and experimental studies of the energy transfer from winds to waves have led to the following parameterization function of wind input [*Plant*, 1982; *Phillips*, 1984, 1985]

$$S_{in}(k) = m\omega\left(\frac{u_*}{c}\right)^2 N(k), \tag{2}$$

where $m \approx 0.04$, $u_*$ the wind friction velocity and $c$ wave phase speed. Following *Phillips* [1984, 1985], the dissipation term is given by

$$S_{ds}(k) = -gk^{-3} f(B), \tag{3}$$

where $B(k) = k^3\chi(k) = k^3\omega N(k)/g$ is the dimensionless wave number spectrum. Equation (2) can be expressed in terms of $B(k)$,

$$S_{in}(k) = m\left(\frac{u_*}{c}\right)^2 gk^{-3} B(k). \tag{4}$$

Examining the functions in (3) and (4), *Phillips* [1984] concludes that the knowledge of the variation of $B(k)$ with $u_*/c$ is critical for advancing our understanding of surface wave dynamics.

[8] For wave components several times shorter than the elevation spectral peak wavelength, experimental data support the following asymptotic equilibrium spectral function

$$\chi_e(k) = bu_* g^{-0.5} k^{-2.5} = b\frac{u_*}{c} k^{-3}. \tag{5}$$

The corresponding dimensionless spectrum is

$$B_e(k) = b\left(\frac{u_*}{c}\right). \tag{6}$$

The range of $b$ has been summarized by many researchers [e.g., *Toba*, 1973; *Phillips*, 1977, 1985; *Forristall*, 1981; *Donelan et al.*, 1985; *Hwang et al.*, 2000]. On the basis of 2D spectral analysis of the 3D topography of an equilibrium surface wave field measured with an airborne scanning lidar system, $b \approx 5.2 \times 10^{-2}$ is reported by *Hwang et al.* [2000]. For short surface waves that are important to ocean remote sensing applications, *Banner et al.* [1989] report wave number spectra measured by stereo photography. The resolved wavelength is from 0.2 to 1.6 m ($4 \le k \le 31$ rad/m), and wind speed from 5.5 to 13.3 m/s. Their results show a very weak spectral dependence on wind speed, $B(k) \sim (u_*/c)^{0.18}$. The analysis of *Hwang and Wang* [2004a] yields result of $B(u_*/c;\ k)$ with a broad coverage in wave number (1 to 314 rad/m) and wind speed (2.6 to 14.2 m/s). Using the wave spectra collected in the ocean by wave gauges mounted on a free-drifting platform, they show that $B$ can be represented by a power law function,

$$B\left(\frac{u_*}{c}; k\right) = A(k)\left(\frac{u_*}{c}\right)^{a(k)}. \tag{7}$$

The magnitude of the exponent $a$ is of special interest because it is also the exponent of the power law function characterizing the wave spectral dependence on wind speed. Analysis of field data reveals a nonmonotonic variation of $a(k)$: the magnitude is close to one for waves longer than about three meters, it drops to about 0.25 in the meter-long spectral range, and gradually increases to about 1.5 at the shorter end of the gravity wave spectrum. The proportionality coefficient $A$ also shows a systematic variation: it has a value approaching (toward low wave number) that of the equilibrium spectral function (0.052), a minimum in the meter-long spectral range, a small hump in the decimeter range, and then slowly rolls off toward higher wave number [*Hwang and Wang*, 2004a, Figure 3; and Figure 2 of this paper to be further discussed later in the next section]. They further divide the spectral data into two subsets depending on the swell influence. The swell index, $S_{var}$, is quantified by the ratio of the spectral densities in the frequency bands $\omega < 0.6\omega_r$ and $\omega \ge 0.6\omega_r$, the reference frequency $\omega_r$ is the higher value between the measured spectral peak frequency, $\omega_p$, and the empirical peak frequency of a fully-developed sea defined as $\omega_0 = g/(1.2U_{10})$. Further discussion on the swell index is described in section 5.1.

[9] The parameters $A$ and $a$ show noticeable difference in the two data groups, particularly, in the swell case the "valley" of $a(k)$ broadens and its minimum shifts toward higher wave number. The change in $A$ is more subtle: with the swell group, there is a slight decrease in higher wave number and increase in lower wave number. Because $c$ and $k$ are related by the wave dispersion relation, $B(u_*/c;\ k)$ can be written as $B(k;\ u_*)$, which becomes a convenient parameterization function of the wave spectrum for ISW. The results of $A$ and $a$ for wind sea and swell influenced conditions are tabulated by *Hwang* [2005] as lookup tables to facilitate computation of $B(k)$ for a given wind speed. In practice, a matrix of $B(u_*/c;\ k)$ is computed for a range of $k$ and $u_*$ using (7). The result is effectively given as $B(u_*;\ k)$, which can be used for describing $B(u_*)$ for a given $k$ or $B(k)$ for a given $u_*$.

### 2.2. Wave Measurement

[10] The empirical determination of $B(u_*/c;\ k)$ is a critical step in this study and it is important to have data that cover a broad range of $u_*/c$. For a given wave number component,

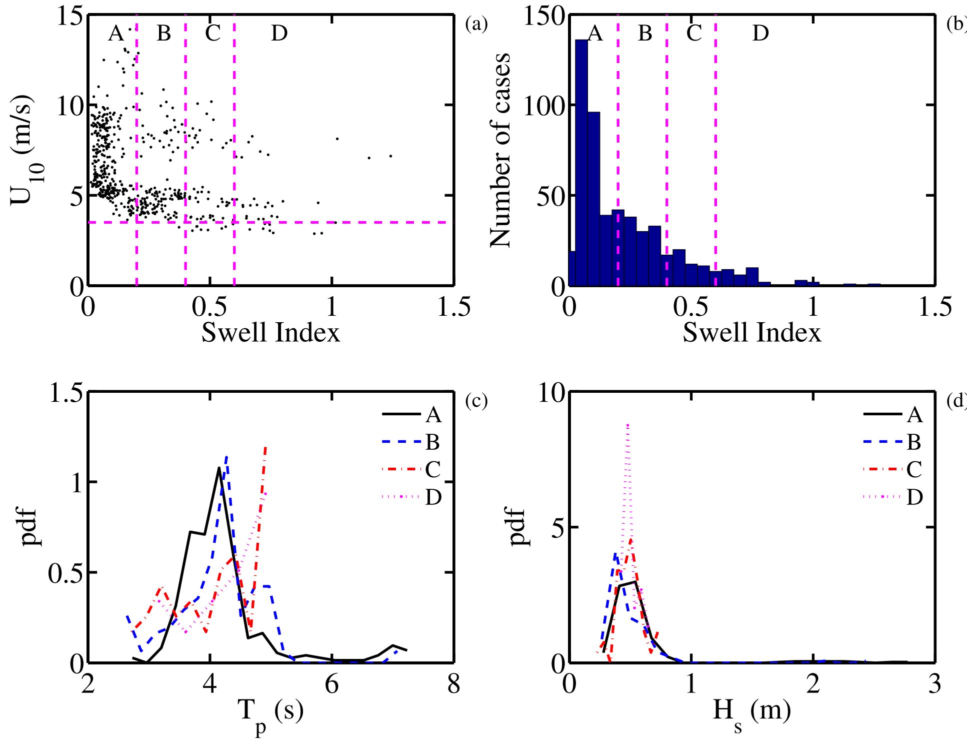


**Figure 1.** Relevant wave conditions in the data set: (a) wind speed range as a function of swell index, (b) histogram of swell index, and pdf of (c) peak wave period and (d) significant wave height.

the range of $u_*/c$ is determined by the range of wind speed. (In order to exclude complications associated with stability effects on wind wave generation, the assembled wave spectra include only near neutral conditions with bulk Richardson number less than 0.02.) The data set is compiled from several separate field experiments conducted between 2001 and 2003 in the Gulf of Mexico. The wave measurement system, the calibration of the wave sensors, and the typical procedure of data acquisition and data processing have been given by *Hwang and Wang* [2004b] so only a brief description is provided here.

[11] A free drifting platform made of open frame aluminum structure is used to carry sensors that measure wind, wave, humidity, and air and water temperatures for air-sea interaction research. All sensors are powered by rechargeable batteries carried on the platform so the system is in free motion once it's deployed in water. A wind vane on the instrument platform ensures its alignment in the wind direction. Effects from buoy's translational and angular motion on the wave measurement are corrected using the output from motion sensors (accelerometers and tilt sensors) mounted on the buoy following the approach given by *Hanson et al.* [1997]. Once release in water, the operation is controlled through a radio link from the tender ship that maintains a distance of about 1 km downwind or crosswind. The duration of each data acquisition episode is between 20 and 40 min. Surface wind velocity is measured by an ultrasonic anemometer at 1 Hz sampling rate. The wind sensor is mounted at about 1.4 m above the mean water level. Surface waves are measured by two linear arrays of wave sensors aligned in the crosswind and upwind directions. Each array has 20 fast response capacitance wave gauges (1 mm diameter thin wires) [*Chapman and Monaldo*, 1995] with a vertical resolution of about 0.2 mm and sampled at 25 or 50 Hz. The spatial interval between the neighboring wire gauges is 0.0508 m. The wind and wave parameters are computed from short data segments of about 2.7 min each. Wave data from the central five wire gauges of the upwind array are used for the discussions in this paper. The degree of freedom is 24 for the spectra from individual wire gauges and 120 for the average spectrum combining all five. Neutral wind speed at 10 m height ($U_{10}$) is calculated from the measured wind speed at 1.4 m height, humidity and air and water temperatures with the application of the method developed by *Liu et al.* [1979] to obtain the dynamic roughness $z_0$ and the logarithmic wind speed profile. Because the complete data set is a collection of several different field experiments with various lengths of deployments and data sampling and processing schemes over a period of about two years, the original spectra are resampled to have uniform frequency resolution with 337 spectral frequency components equally distributed between 0.5 and 75 rad/s. Most of the experiment sites are located between 30 and 60 km offshore in the northern part of Gulf of Mexico with local depth greater than 20 m and the ISW are in deep water wave condition.

### 2.3. Swell Partition

[12] Figure 1a illustrates the wind speed distribution as a function of the swell index, $S_{var}$. There is a reasonably wide range of wind speed coverage for a given $S_{var}$ range. The data are divided into four bands of $S_{var}$ coverage (identified as A, B, C and D bands). The first three bands have an equal

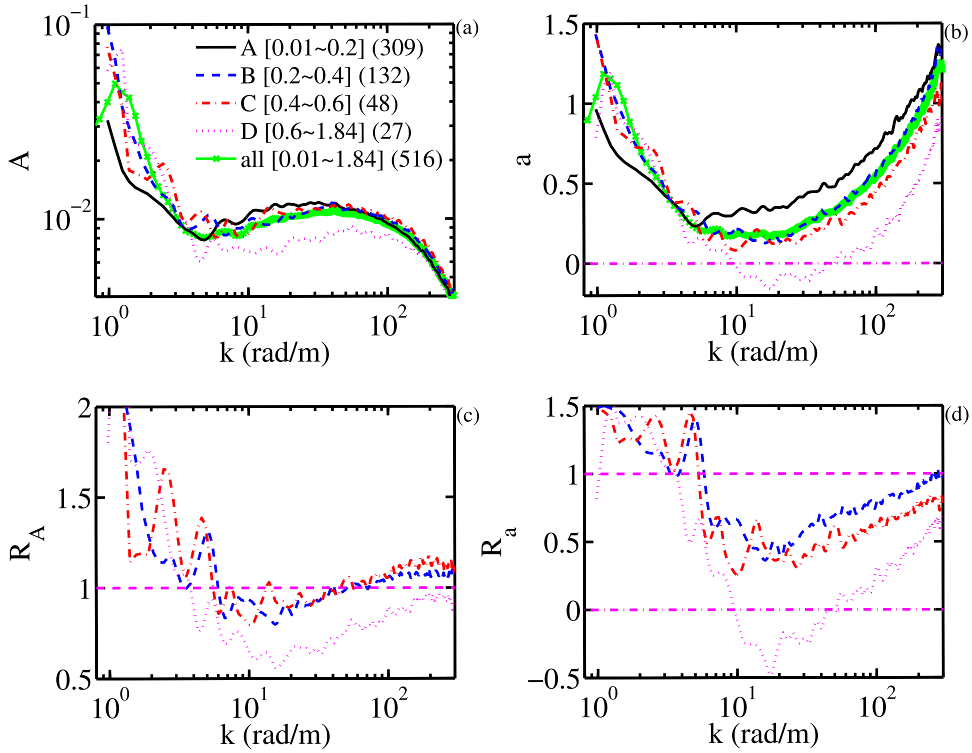


**Figure 2.** (a) Proportionality coefficient $A$ and (b) exponent $a$ of the power law dimensionless spectral parameterization for four different swell conditions; ratio of the spectral parameterization coefficients of the swell influenced conditions and the reference: (c) $R_A$ and (d) $R_a$. In the figure legend of Figure 2a, the range of the swell index in each band is shown in square brackets, and the number of spectra in the band is shown in parentheses.

bandwidth of 0.2 and the fourth includes all cases with $S_{var} > 0.6$. The histogram of the swell index is shown in Figure 1b. Empirically, it is found that excluding data with wind speeds less than 3.5 m/s improves the polynomial fitting of the power law function $B(u_*/c)$ (7). The numbers of spectra in A, B, C and D bands used in the analysis are 301, 132, 48 and 27, respectively. The range of coverage of peak wave period, $T_p$, and significant wave height, $H_s$, in the four bands are reasonably broad, their probability density functions (pdf) are shown in Figures 1c and 1d. In the subsequent discussions band A is the reference ocean wave condition with least swell effect, and B, C, D are conditions with increasing swell influence.

## 3. Spectral Parameterization and Swell Influence

[13] As described in section 2, the dependence of the dimensionless wave spectrum, $B(k)$, on the dimensionless wind friction velocity, $u_*/c$, follows a power law relation (7). Applying the analysis procedure to the data in the four swell index bands, the proportionality coefficient, $A$, and exponent, $a$, of the power law function are shown in Figures 2a and 2b, respectively. The progressive variation of the power law parameters with increasing swell index can be easily detected. For reference, the average results of $A$ and $a$ processed with all spectra without sorting out the swell influence are also shown: for the assembled data, they are very similar to those of swell index band B.

[14] The physical meaning of $A$ and $a$ can be better appreciated by rewriting (7) as

$$B(k) = g^{-0.5a} k^{0.5a} A u_*^a. \tag{8}$$

In this presentation, it is clear that $A$ is a critical element of the shape factor of the dimensionless spectrum, $B$: the spectral slopes (with respect to $k$) of $A$ and $B$ differ by a magnitude equal to $0.5a$. As discussed in section 2, $a$ is the exponent of the power law spectral dependence on wind speed. In the equilibrium range a linear wind speed dependence is expected, (6). The exponent from ISW processing is suggestive of approaching this asymptotic value toward the low wave number (Figure 2b). The exponent has a smooth and nonmonotonic variation with wave number. For the reference case (band A), the wind speed dependence gradually decreases to a minimum of 0.23 near $k$ = 5 rad/m and then increases more gradually to 1.3 at $k$ = 300 rad/m, similar to the results reported by *Hwang and Wang* [2004a].

[15] Both $A$ and $a$ of B, C, and D bands show gradual departure from those of the reference A band. There is a nodal point near $k$ = 3 rad/m where their magnitudes remain almost constant for all four bands. The significance of the nodal point wave number is not fully clear at this point but related research seems to suggest a close association with the dominant length scale of surface wave breaking [*Hwang*, 2007; *Hwang et al.*, 2008a, 2008b]. Overall, the curves of $A(k)$ and $a(k)$ rotate clockwise pivoting around the

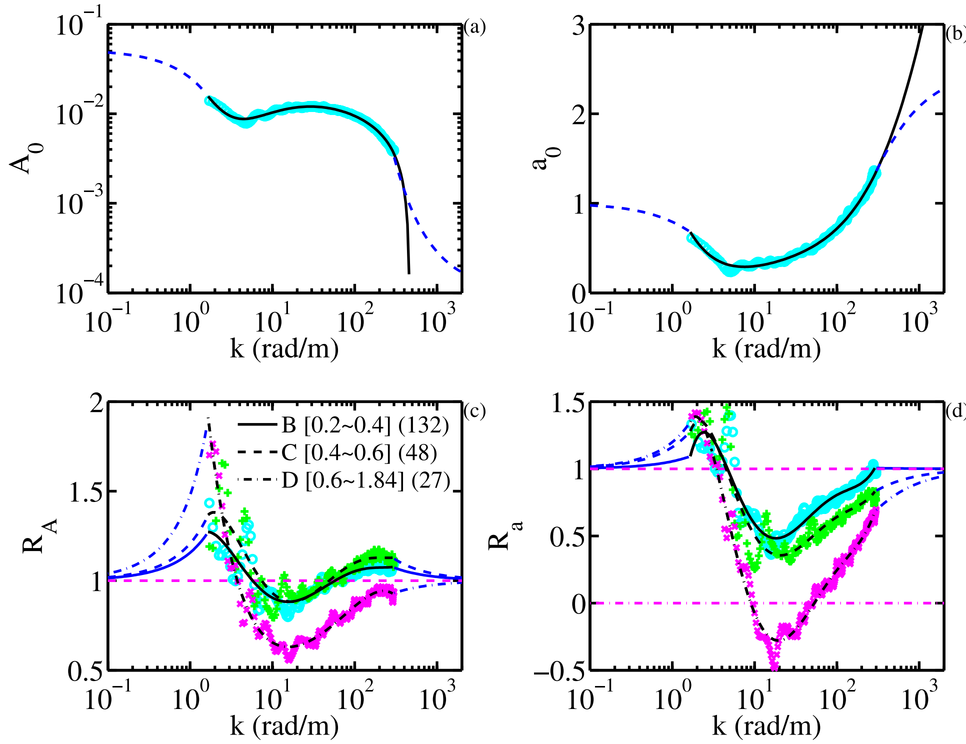


**Figure 3.** Polynomial fitting results and analytical extension of (a) $A_0$, (b) $a_0$, (c) $R_A$, and (d) $R_a$ for the purpose of computing the ocean surface roughness spectrum.

nodal point as the swell index increases. With increasing swell influence, $A$ and $a$ decrease toward higher wave number. Toward lower wave number, the trend reverses but the increment in $A$ and $a$ is much less dependent on the swell influence compared to the decrement in the high-wave number region. With large enough swell influence, $a$ may become negative. This is an important feature because at $a(k) = 0$ the spectral density in the corresponding wave number range saturates and the information of wind speed dependence no longer exists. The wave spectra derived from the parameterization function will be further discussed in section 4.

[16] To facilitate spectral computation, polynomial equations for $A(k)$ and $a(k)$ are obtained with least square fitting. With subscript 0 representing the reference case (band A), the following notation is adapted:

$$A(k) = R_A(k)A_0(k), \tag{9}$$

and

$$a(k) = R_a(k)a_0(k). \tag{10}$$

The ratio $R_A$ and $R_a$ derived from the experimental data of B, C and D bands with respect to the reference condition (A band) are illustrated in Figures 2c and 2d. Fifth-order polynomial fitting coefficients for $A_0$, $a_0$, and $R_A$ and $R_a$ for the B, C and D bands are listed in Table 1, only data within the range $1.5 \leq k \leq 300$ rad/m are included in the polynomial data fitting with consideration of the most restrictive wave number coverage in the D band (see section 5.2 for further discussions). The comparison of fitted curves and field measurements is shown in Figure 3.

[17] For the purpose of computing the mss, spectral functions need to be modeled for the low- and high-wave number regions not covered by the field data. As discussed earlier [*Hwang*, 2005, *Hwang*, 2008] the dominant contributor of integrated mss is from the ISW, so simple analytical functions are used here to extend $A(k)$ and $a(k)$ into the low- and high-wave number regions. The following factors are considered for the design of the analytical functions: (1) $A_0$ and $a_0$ approach their corresponding values of the equilibrium spectrum (6) toward low wave number, that is, $A_0$ $(k \to 0) = 0.052$ and $a_0$ $(k \to 0) = 1$. (2) Swell influence

**Table 1.** Coefficients of the Polynomial Fitting Equation, $Y = \sum_{n=0}^{N} P_n\, k^{N-n}$, Where $Y$ is the Parameter Shown in the First Column

| | $P_0$ | $P_1$ | $P_2$ | $P_3$ | $P_4$ | $P_5$ |
|---|---|---|---|---|---|---|
| $A_0$ | −3.862e−5 | 7.991e−4 | −6.417e−3 | 2.342e−2 | −3.668e−2 | 2.898e−2 |
| $a_0$ | −5.213e−4 | 1.524e−2 | −1.358e−1 | 5.865e−1 | −1.167e+0 | 1.136e+0 |
| $R_A$ (B) | 2.811e−3 | −4.911e−2 | 3.040e−1 | −7.542e−1 | 5.349e−1 | 1.159e+0 |
| $R_a$ (B) | 1.127e−2 | −1.948e−1 | 1.241e+0 | −3.443e+0 | 3.683e+0 | −3.779e−2 |
| $R_A$ (C) | 4.258e−3 | −7.628e−2 | 4.905e−1 | −1.310e+0 | 1.176e+0 | 1.049e+0 |
| $R_a$ (C) | 9.373e−3 | −1.645e−1 | 1.057e+0 | −2.907e+0 | 2.855e+0 | 4.543e−1 |
| $R_A$ (D) | −2.318e−3 | 4.107e−2 | −3.092e−1 | 1.278e+0 | −2.769e+0 | 3.024e+0 |
| $R_a$ (D) | 1.384e−2 | −2.394e−1 | 1.512e+0 | −4.019e+0 | 3.569e+0 | 3.932e−1 |

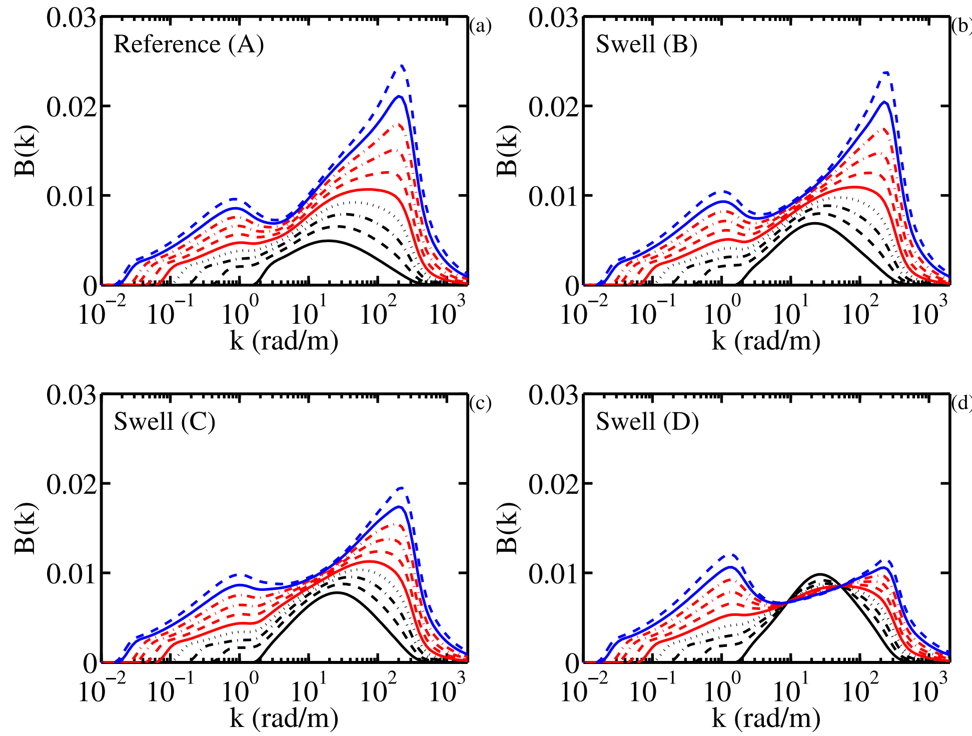


**Figure 4.** (a) Dimensionless spectra calculated for wind speed from 2 to 20 m/s in 2 m/s steps: (a) reference condition (A band swell index), (b) B band, (c) C band, and (d) D band.

on the spectral density decreases toward both low- and high-wave number regions, that is, $R_A$ ($k \to 0$) = 1, $R_a$ ($k \to 0$) = 1, $R_A$ ($k \to \infty$) = 1, and $R_a$ ($k \to \infty$) = 1. (3) The analytical functions maintain continuity with the fitted polynomial equations for the wave number range $1.5 \leq k \leq 300$ rad/m. (4) On the basis of measurements of radar cross sections at various frequencies and incident angles [e.g., *Masuko et al.*, 1986; *Phillips*, 1988; *Weissman et al.*, 1994; *Colton et al.*, 1995], the exponent of the power law wind speed dependence of the corresponding Bragg waves changes from about 0.5 at $k$ = 10 rad/m to between square and cubic at $k > 500$ rad/m [*Hwang*, 1997, Figure 5]. The asymptotic value of $a_0$ for $k \to \infty$ is set at 2.5. (5) The asymptotic value of $A_0$ toward large wave number is more difficult to establish. Direct extension of the fitted polynomial equation shows an unrealistically sharp drop beyond $k$ = 300 rad/m. In the present modeling effort, $A_0$ ($k \to \infty$) = $10^{-4}$ is used. A sensitivity test is conducted using several different asymptotic values. Because the mss contribution from high-wave number region is small, the difference is negligible in comparison to the scatter of mss data.

[18] An exponential function is chosen for the analytical extension. For the low wave number ($k$ < 1.5 rad/m), the function is given as

$$y = Q\exp(qk), \tag{11}$$

where $y$ is $A_0$, $a_0$, $R_A$ or $R_a$. $Q$ and $q$ are solved with the boundary conditions at $k = k_0$ and $k_1$ (0 and 1.5 rad/m in the present case) as defined above. Denoting the boundary values as $y_0$ and $y_1$, then $Q = y_0$ and $q = \ln(y_1/y_0)/k_1$.

[19] For the high-wave number extension ($k$ > 300 rad/m), the function is given as

$$y = P\exp(p/k). \tag{12}$$

$P$ and $p$ are solved with the boundary conditions at $k = k_2$ and $k_\infty$ (300 and $\infty$ rad/m in the present case) as defined above. Denoting the boundary values as $y_2$ and $y_\infty$, then $P = y_\infty$ and $p = k_2\ln(y_2/y_\infty)$. These extension functions are shown in Figure 3 together with the fitted polynomial equations.

## 4. Roughness Spectrum and Mean Square Slope

### 4.1. Dimensionless Spectrum

[20] The dimensionless wave number spectra calculated for wind speeds from 2 to 20 m/s in steps of 2 m/s are shown in Figure 4. Because $B(k) = k\chi_1(k)$, where $\chi_1(k)$ is the surface slope spectrum, with the semilogarithmic plot of Figure 4 the area under the curve for a given wave number range is the integrated mss. For the reference condition A, the dominance of mss contribution from the ISW ($1 \leq k \leq 300$ rad/m) is obvious. As swell influence increases, the portion of mss from the higher-wave number region of ISW decreases and that from lower wave number components becomes more important. The nodal point near $k$ = 3 rad/m in $A(k)$ and $a(k)$, as shown in Figure 2, marks the approximate separation point of swell enhancement or suppression of the spectral surface roughness but the dependence of $B(k)$ on swell influence is a complex function of wave number and wind speed to be further discussed in section 4.3.

[21] For strong swell influence, the variation of the spectral density becomes insensitive to wind speed in the wave number region between about 7 and 70 rad/m. It can be

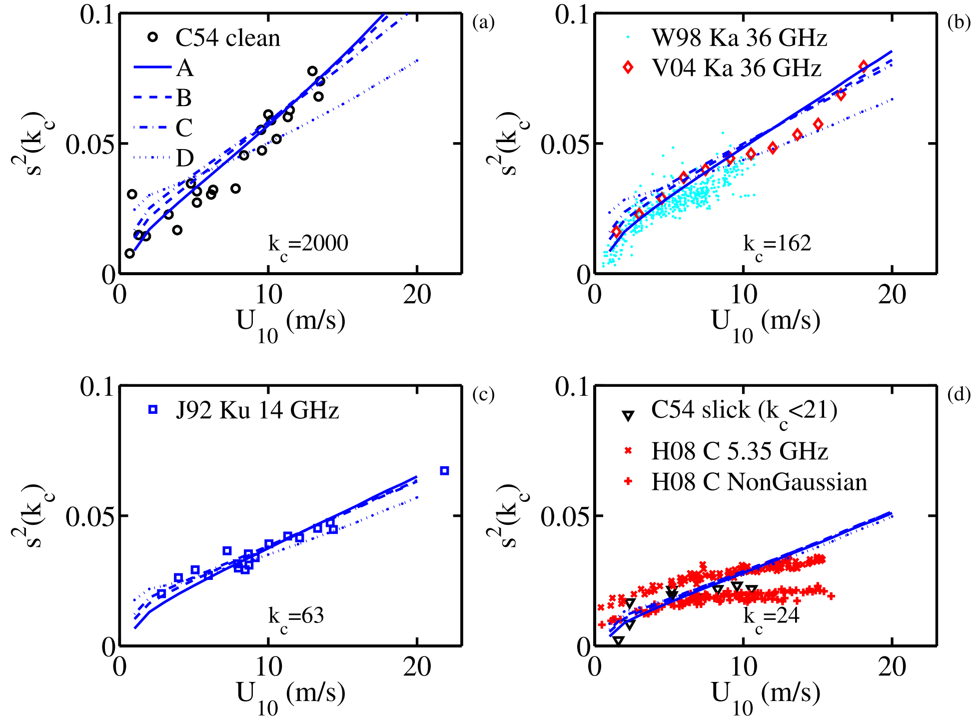


**Figure 5.** Integrated mean square slope and comparison with field data: (a) $k_c$ = 2000 rad/m and the clean water sun glitter data of *Cox and Munk* [1954], (b) $k_c$ = 162 rad/m and Ka band radar data of *Walsh et al.* [1998] and *Vandemark et al.* [2004], (c) $k_c$ = 63 rad/m and Ku band radar data of *Jackson et al.* [1992] (including data of *Jones et al.* [1977] and *Wentz* [1977]), and (d) $k_c$ = 24 rad/m and slick water sun glitter data of *Cox and Munk* [1954] and C band radar data of *Hauser et al.* [2008].

inferred that under such conditions (large swell and Bragg wave number between about 7 and 70 rad/m) the observed variation of the radar cross section with wind speed is mainly due to the tilting effect by surface waves longer than the Bragg waves, the direct effect of the dependence of Bragg wave spectral density on wind speed is probably negligible or even counteracting the tilting effect.

### 4.2. Mean Square Slope

[22] With the wave spectrum established, the mss integrated to a given wave number can be carried out. The integrated mss can be compared with those measured by remote sensing techniques with different EM frequencies. There are now several large data sets reported in the literature. The resolved wave number range varies from optical [*Cox and Munk*, 1954; including clean water and natural or artificial slicks] to the tilting wave components at Ka (36 GHz) [*Walsh et al.*, 1998; *Vandemark et al.*, 2004], Ku (14 GHz) (*Jackson et al.* [1992]; including data by *Jones et al.* [1977]and *Wentz* [1977]) and C band (5.35 GHz) [*Hauser et al.*, 2008] radars in altimeter mode of application. The procedures to retrieve the mss from remote sensing measurements are quite complex and exhaustive discussions have been given in the source papers and the references therein so they are not repeated here. Figure 5 displays the comparison of these remote sensing measurements with the results integrated from the spectra described earlier. The upper bound cutoff wave number, $k_c$, for integration is determined by the radar wave number, $k_r$. The criterion $k_c = k_r/4.7$ suggested by *Jackson et al.* [1992] is adapted here. The calculated $k_c$ for Ka, Ku and C band radar waves are 162, 63 and 24 rad/m, respectively. For the clean water case of the optical measurement, the integration is carried to $k_c$ = 2000 rad/m. For the slicked water case $k_c$ is set at 21 rad/m based on the description by *Cox and Munk* [1954] that waves shorter than 0.3 m are suppressed by the slicks. The agreement of the mss derived from remote sensing and spectral integration is generally very good for higher-cutoff wave numbers that include more ISW components (Figures 5a to 5c).

[23] For mss with lower cutoff wave numbers, as in the C band radar and slick water cases, the agreement is fair. The cutoff wave number of C band and slick cases are very similar and the data are grouped together in Figure 5d. The analyses of *Hauser et al.* [2008] produce two sets of mss with the assumption of Gaussian (shown in their Figure 5d) and non-Gaussian (their Figure 11b) surface slope pdf. They have noticed the large difference between the two mss sets but offered no explanation. Both C band mss sets are included in the figure. As will be explained in section 5.2, the result of the low-wave-number spectral parameterization is expected to be less accurate because of the reduced data points available. Further improvement requires expanding the experimental database to increase the reliability of the spectral parameterization in the low-wave-number region.

[24] On the other hand, acquiring low-wave-number surface slope data is a very challenging task. As shown in Figure 5d, a significant offset of mss at null wind speed is found in either set of C band mss, strongly suggesting the presence of contribution from nonlocal wind source in their

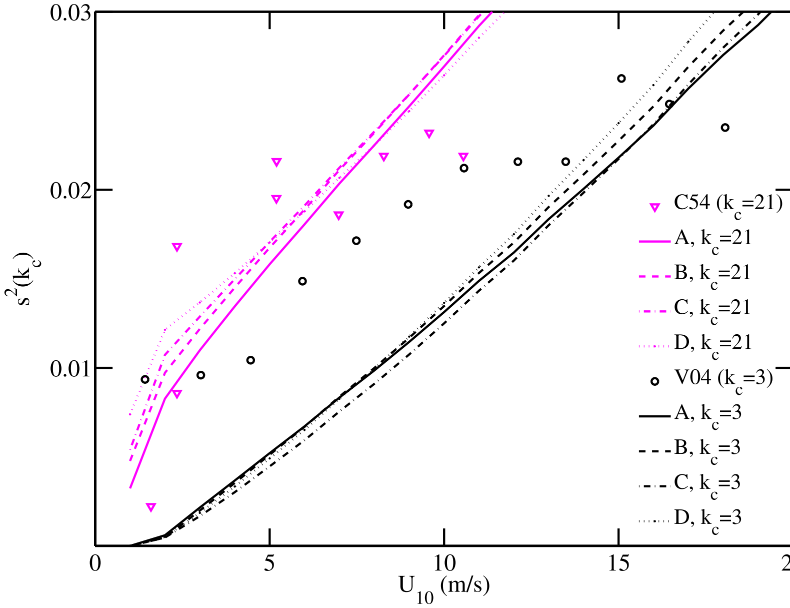


**Figure 6.** Mean square slope integrated to $k_c$ = 3 rad/m and comparison with the laser altimeter data of *Vandemark et al.* [2004]. For reference, the slick water sun glitter data of *Cox and Munk* [1954] and integrated mss with $k_c$ = 21 rad/m are also shown in lighter color.

wave condition. To make the discussion of mss dependence on wind speed meaningful, the nonlocal contribution needs to be removed from the processed result. *Hauser et al.* [2008] do not provide much information about the wind and wave conditions of their experiment. On the basis of the tabulated data of the same experiment presented in an earlier paper [*Mouche et al.*, 2005], the wave fields are indeed strongly influenced by swell not related to local wind conditions. A more detailed discussion of this issue is given by *Hwang* [2008]. The difficulty of obtaining uncontaminated mss in the low-wave-number region for investigating the wind speed dependence is also seen in the laser altimeter data presented by *Vandemark et al.* [2004]. The data are collected with three laser altimeters arranged in an equilat-

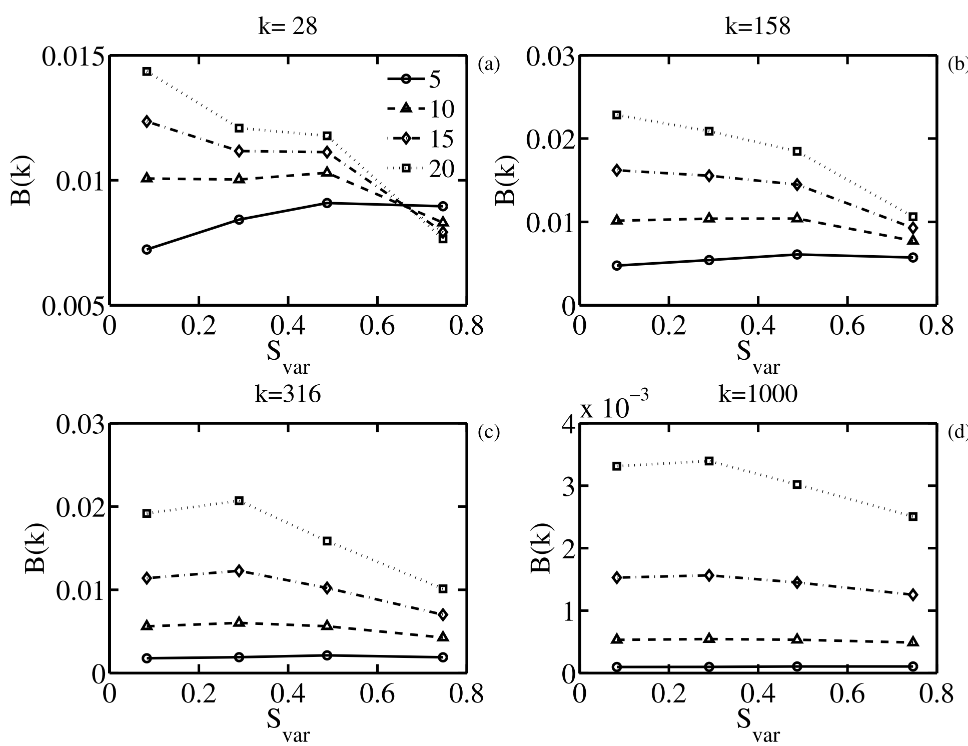


**Figure 7.** Swell effect on the Bragg component of the ocean surface roughness at four spectral wave number components corresponding to approximately (a) L, (b) C, (c) Ku or X, and (d) Ka band radar frequencies; wind speeds 5, 10, 15, and 20 m/s are shown.

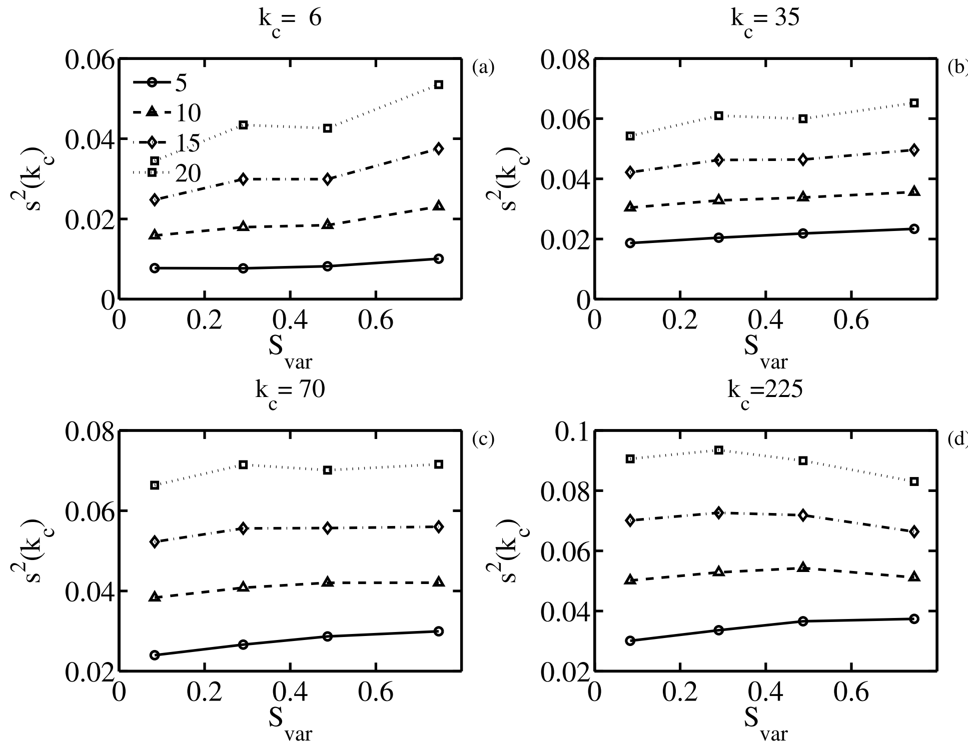


**Figure 8.** Same as Figure 7 but for the tilting component of surface roughness.

eral triangle with 0.95 m spacing and carried on a low-flying aircraft. The resolved sea surface slope has an upper cutoff wave number of about 3 rad/m. Figure 6 shows the comparison of the laser altimeter data set (black circle) with the mss integrated from the spectral model (black curves). A conspicuous mss offset at low wind speed is also evident in the laser altimeter measurement and reveals the wave contribution not related to local wind. It highlights the difficulty of removing nonlocal contribution in the low-wave-number mss for investigating its wind speed dependence. If a constant level of about 0.008 is subtracted from the laser altimeter mss, the agreement with the model mss is actually quite impressive, at least for $U_{10}$ less than about 10 m/s. For reference, the slick data of *Cox and Munk* [1954] are also shown in the figure with light-colored triangle. The trend of the slick mss data shows a critical wind speed for wind wave generation, rather than the preexistence of wave motion in the absence of wind as in the laser and C band data. Given the large data scatter, the agreement of slick data with model mss (light colored curves) is also quite good.

[25] Taking into consideration the problem of removing nonlocal contribution in the low-wave-number mss data, it seems that the simple asymptotic approach described in section 3 to extend the wave number range of the modeled dimensionless spectrum captures the main essence of the ocean surface roughness spectral composition even in the low-wave-number region.

### 4.3. Swell Influence

[26] For radar applications, two partitions of the surface roughness are of special interest: the Bragg resonant component and the titling component. The former refers to a narrow band of the roughness spectrum in the neighborhood of $k = 2k_r \sin\theta_i$, where $\theta_i$ is the radar incident angle. The latter refers to the roughness spectral components longer than several times (on the order of about five) of the Bragg wavelength. At moderate incident angles (about 20 to 60°), Bragg resonance is the major contributor of radar backscatter. Tilting roughness modifies the actual (local) incident angle that the radar views the scattering roughness. Radar backscatter intensity varies strongly with incident angle and Bragg wavelength varies at different phases of long waves for a given nominal incident angle, computation based on local incident angle is important [e.g., *Wright*, 1966, 1968].

[27] Figure 7 displays the swell influence on the Bragg waves at approximately L, C, Ku (and X), and Ka band radar frequencies for wind speeds 5, 10, 15 and 20 m/s. The nominal values for the relevant parameters used in presenting Figures 7 and 8 are listed in Table 2. In this figure, $S_{var}$ on the abscissa are the average swell indices in the four bands of field data. The wave number range in the present modeling effort is logarithmically distributed so the nearest wave number is shown to represent the Bragg waves. The Bragg roughness of L band, and C and Ku bands to a lesser extent, is severely impacted by the swell, as expected from the spectra shown in Figure 4, where large variation in the

**Table 2.** Nominal Values of L, C, X, Ku, and Ka Band Radar Frequencies and the Corresponding Bragg and Tilting Wave Numbers Used for Figure 7 and 8

| | $f_r$ (GHz) | $\lambda_r$ (m) | $k_r$ (rad/m) | $k_{\mathrm{Bragg}}$ (rad/m) | $k_{\mathrm{TiltScat}}$ (rad/m) | $k_{\mathrm{TiltAlt}}$ (rad/m) |
|---|---|---|---|---|---|---|
| L | 1.0 | 0.300 | 21 | 29 | 6 | 4 |
| C | 5.5 | 0.055 | 115 | 161 | 34 | 25 |
| X | 10.0 | 0.030 | 209 | 293 | 62 | 45 |
| Ku | 14.0 | 0.021 | 293 | 411 | 87 | 62 |
| Ka | 36.0 | 0.008 | 754 | 1056 | 225 | 160 |

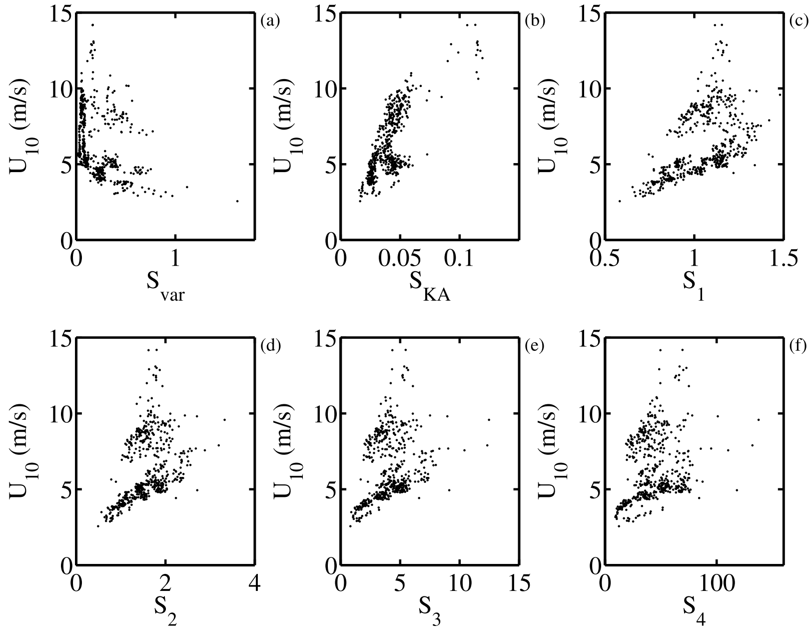


**Figure 9.** Wind speed range with respect to different definitions of swell index: (a) variance ratio between low- and high-frequency waves, (b) steepness of low-frequency waves, and (c–f) first to fourth moments of wave spectrum.

wind speed dependence of wave spectrum on the swell index is seen in the range of wave numbers between about 7 and 70 rad/m. The wind speed dependence almost vanishes near $S_{var}$ = 0.6.

[28] The swell response of Bragg roughness of a given wave number component is wind speed dependent. At low wind the Bragg spectral density increases more or less monotonically with the swell intensity. The trend reverses for wind speed greater than about 10 m/s. As swell influence increases, the wind speed dependence of a Bragg wave component decreases.

[29] Figure 8 shows the swell influence on the tilting surface waves at approximately L, C, Ku (and X), and Ka band radar frequencies. (The integrated mss is interpolated with cubic spline fit to equal wave number spacing of 1 rad/m.) In most cases, there is a generally increasing trend of the mss with swell index except at high radar frequency with moderate and high wind (Ka band, Figure 8d). Because the tilting roughness integrates over a wide range of wave number components, the upper region suppressed and lower region enhanced by swell, the overall variation with swell index is much milder than the effect on the narrow band Bragg component.

## 5. Discussions

### 5.1. Swell Index

[30] By definition, swell is wave motion not generated by local wind. Even with directional wave spectrum, identification of swell components is a challenging task [e.g., *Hanson and Phillips*, 2001]. In the absence of directional information, the only reliable parameter is the wave frequency. (During a few of the deployments, the compass orientation was not aligned properly and the swell directional information becomes unusable in the assembled data set.) Some obvious properties of low-frequency waves that can be used to quantify the swell effects include the steepness ($S_{KA}$), the spectral variance ($S_{var}$), and the spectral bandwidth defined by the spectral moments ($S_n$). The $n$-th spectral moment in this application is rendered dimensionless by normalizing with $\omega_p^n$. In the present study, establishing the power law relationship of $B(u_*/c)$ requires that whatever the swell index is chosen, the different swell bands contain a wide range of wind speeds to facilitate a more reliable data fitting to obtain the power law parameters. Thus the parameter $c_p/U_{10}$ for a swell index as employed by *Hwang and Shemdin* [1988] is not considered here because it would obviously truncate the wind speed range in each swell index band because of the $U_{10}$ factor. Figure 9 shows the distributions of wind speeds in the collected data set as a function of several candidates of swell index discussed above. $S_{var}$ is selected because of the more uniform wind speed distribution. In the future when large data sets with good coverage of wind speed are available, a more sophisticated definition of the swell index may be more desirable.

### 5.2. Low-Wave-Number Components of ISW

[31] In the collection of spectra, the majority are with multiple local peaks. The procedure to derive the peak wave frequency follows the suggestion by *Young* [1995],

$$\omega_p = \frac{\int_0^\infty \omega \chi^4(\omega) d\omega}{\int_0^\infty \chi^4(\omega) d\omega}. \tag{13}$$

No attempt is made to separate single peak and multi-peak spectra because of two main reasons: (1) To have a wider range of wind speeds for more accurate spectral parameterization; and (2) Wind forcing applies to all wave components that are moving slower than about $1.2U_{10}$ regardless of the spectral shape of single or multiple peaks. The conditions A,

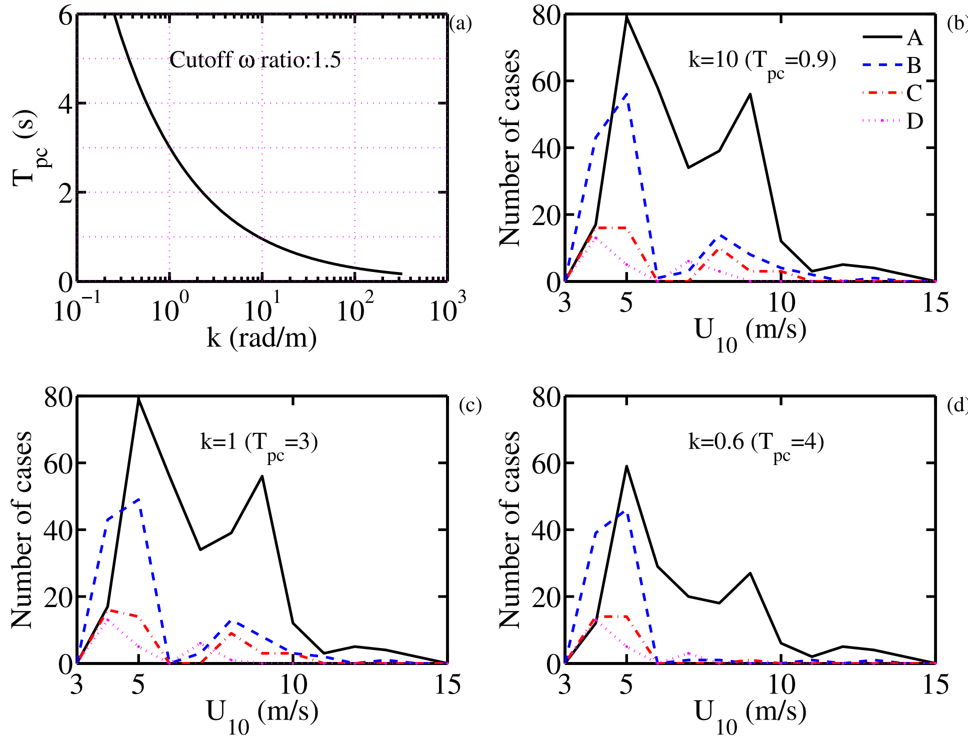


**Figure 10.** (a) Minimum peak wave period as a function of the corresponding minimum wave number of the spectral components included in the spectral parameterization analysis and the wind speed histogram of the spectra used for wave component $k$ at (b) 10, (c) 1, and (d) 0.6 rad/m.

B, C and D are thus all mixed seas but with different levels of swell influence. The ISW components are usually located in the region far away from the spectral peaks except for the lower wave number components at low wind velocity (say, $k < 1$ rad/m, which corresponds to $\omega < 3$ rad/s approximately). In the data processing of spectral parameterization, a criterion is set to include only spectral components satisfying $\omega/\omega_r > 1.5$ to ensure that only wind generated wave components are processed. This criterion results in excluding more low-wind-speed cases toward lower wave number as a result of increased minimum peak wave period of the wave spectrum selected for data processing (Figure 10a). Examples of the wind speed histogram of $k = 10$, 1 and 0.6 rad/m for the four swell index bands are displayed in Figures 10b to 10d. The quality of the processed result is expected to deteriorate toward the very low wave number range of ISW (say, $k < 1$ rad/m) because of the significant reduction in the available data quantity and wind speed range. For wave components with $k \geq 1$ rad/m (the focus of discussion in this paper), the wind speed range for spectral parameterization fitting is essentially the same (Figures 10b and 10c).

### 5.3. Limitation of the Present Data Set

[32] The specific range of surface wind and wave conditions that define swell impact in the present data set is rather limited. The analysis presented in Figures 1 and 10 helps to bring this into focus. It shows first that the swell-dominated cases sampled are very few in this data set. Also, the significant wave height is very low in all cases of this study (Figure 1d). It is notoriously difficult to acquire enough field data in wind/wave studies to call a given data set "representative". The limited range of field conditions for the whole of the study do not even slightly approach open ocean conditions where the significant wave height is almost always above 1 m and more typically lies at 2 to 3 m. Thus while many spectra may have been measured and the degree of freedom (DOF) of spectral analysis is high (accurate spectra), the range of conditions encountered is too low to call the results generally representative. This suggests a very low geophysical DOF to support the study's conclusions with the ISW wave spectral data alone.

[33] On the other hand, several critical features in this study can be detected in other independent field experiments under wind and wave conditions much more representative of the open ocean. For example, *Hwang and Wang* [2004a] extend the ISW analysis to derive the breaking dissipation source term from the spectral parameterization function following the approach of *Phillips* [1984]. They conclude that the shifting of the "distribution valley" of exponent $a$ toward higher wave number in mixed seas corresponds to shifting of wave breaking to shorter length scale due to swell impact. This feature is also found in the more direct measurements of wave breaking using radar sea spike analyses [*Frasier et al.*, 1998; *Hwang et al.*, 2008a, 2008b]. The radar frequency in both experiments is X band with a radar wavelength of about 3 cm. The experiment of *Frasier et al.* [1998] is conducted onboard the floating instrument platform (FLIP) in the Pacific Ocean at a location about 50 km west of Monterey, California. The range of wind speed is from 3 to 15 m/s and significant wave height from 1 to 4 m. The experiment of *Hwang et al.*

[2008a, 2008b] is conducted on a tower in the Atlantic Ocean, located about 60 km offshore of the east coast of Georgia. The range of wind speed is from 7 to 15 m/s and significant wave height from 1.2 to 2.7 m. The results from both experiments show a prominent reduction of the breaking length scale with stronger swell presence in the wave field. In the analysis of the latter experiment, *Hwang et al.* [2008b] also show that the radar backscattering cross section is reduced by the swell, which suggests that the ocean surface roughness in the centimeter length scale is reduced by the swell (in comparison to the wind sea condition), which is another key feature of the present analysis of swell impact on ocean surface roughness spectrum.

[34] Another concern is that the wind friction velocity is derived using a bulk formula from wind measurements at 1.4 m above the surface. This parameter's accuracy and its independence from the swell seem to be key assumptions in the study. There is a large body of field studies that show the friction velocity magnitude and direction can be impacted by swell or seas. In effect, there is air-sea coupling going on that may cause $u_*$ to deviate from a bulk estimator depending on the direction of the swell system with respect to the mean wind flow. Unfortunately, the sensors on the free drifting platform are optimized for ISW measurements and only basic for wind stress estimation. The effort to investigate the swell impact on $u_*$ is further hampered by the problem in the compass misalignments as mentioned in section 5.1. Intuitively, whether the swell increases or decreases $u_*$, the effect also results in an increase or decrease in $B(k)$. This would create a self correcting effect as far as deriving the empirical power law relation of $B(k;\ u_*/c)$ is concerned. However, it is true that in future experiments of ISW measurement, more attention should be paid to wind stress acquisition (and vice versa).

## 6. Summary

[35] Field measurements of the ocean surface wave spectra focusing on the slope-contributing components are analyzed to establish an ocean surface roughness spectral model. The spectral parameterization is based on the empirical power law relation between the dimensionless wave spectrum and wind speed. Experimental data reveal that the power law parameters (the proportionality coefficient and exponent) are modified by the swell. The swell influence is quantified with the field data in this paper.

[36] The close association between the power law parameters with the spectral property and characteristics of wind wave generation is discussed in section 3. In particular, $a$ represents the exponent of the power law dependence of the wave spectral density on wind speed. For ISW of the reference condition (minimum swell influence), the wind speed dependence shows a nonmonotonic variation with wave number: having a value of about one in the low-wave-number end of ISW ($k$ = 1 rad/m), decreasing to a minimum of about 0.23 near $k$ = 5 rad/m and then increasing to about 1.3 at $k$ = 300 rad/m (Figure 2b). As the swell influence increases, the local minimum of $a(k)$ moves toward higher wave number and the valley region broadens, reflecting the shifting of breaking process toward broader and shorter length scales [*Hwang and Wang*, 2004a; *Frasier et al.*, 1998; *Hwang et al.*, 2008a, 2008b]. The magnitude of the local minimum also decreases and may become negative for very large swell index, signifying the reduced dependence on wind speed of the decimeter-scale ISW in increasing swell influence.

[37] A design of the analytical extension of the power law parameters to both low- and high-wave number regions outside the field data range is presented. The swell effects on the resulting spectra are described in section 4. The integrated mss are compared with those obtained by remote sensing techniques with EM frequencies ranging from optical to Ka (36 GHz), Ku (14 GHz) and C (5.35 GHz) band radars, as well as a data set collected by airborne laser altimeters spaced about one meter apart in an equilateral triangle. The agreement is very good for those with larger contributions from the ISW (optical, Ka and Ku bands) but fair for those weighted toward low wave number. The result indicates the need to improve our understanding of the wave properties in the lower wave number range of the ISW. It also highlights the importance in incorporating the swell parameter in the analysis of surface roughness properties using remote sensing methods that employ lower radar frequencies, say below 10 GHz, or other techniques that address the low-wave-number contributions such as wide spacing sensor arrays.

[38] **Acknowledgments.** This work is sponsored by the Office of Naval Research (NRL program element 62435N and 61153N; NRL contribution NRL/JA/7260-08-0241). Two anonymous reviewers provided constructive suggestions and careful reading of the manuscript. Reviewer 2 also offered several insightful comments regarding the placing of the present work in the larger context of previous studies and the concerns of limited range of parameters in the study conditions restricting the generality of resulting conclusions. Section 5.3 outlines his/her major concerns and the relevant discussions.

## References

Apel, J. R. (1994), An improved model of the ocean surface wave vector spectrum and its effects on radar backscatter, *J. Geophys. Res.*, *99*, 16,269–16,291.

Banner, M. L., I. S. F. Jones, and J. C. Trinder (1989), Wavenumber spectra of short-gravity waves, *J. Fluid Mech.*, *198*, 321–344.

Bjerkaas, A. W., and F. W. Riedel (1979), Proposed model for the elevation spectrum of a wind-roughened sea surface, *Tech. Rep. APL-TG-1328-1-31*, 31 pp., Applied Physics Laboratory, Johns Hopkins Univ., Laurel, Md.

Chapman, R. D., and F. M. Monaldo (1995), A novel wave gauge sensor, *J. Atmos. Ocean. Technol.*, *12*, 190–196.

Colton, M. C., W. J. Plant, W. C. Keller, and G. L. Geernaert (1995), Tower-based measurements of normalized radar cross section from Lake Ontario: Evidence of wind stress dependence, *J. Geophys. Res.*, *100*, 8791–8813.

Cox, C. S., and W. Munk (1954), Statistics of the sea surface derived from sun glitter, *J. Mar. Res.*, *13*, 198–227.

Donelan, M. A. (1987), The effect of swell on the growth of wind waves, *APL Tech. Dig.*, *8*, 18–23.

Donelan, M. A., and W. J. Pierson (1987), Radar scattering and equilibrium ranges in wind-generated waves with application to scatterometry, *J. Geophys. Res.*, *92*, 4971–5029.

Donelan, M. A., J. Hamilton, and W. H. Hui (1985), Directional spectra of wind-generated waves, *Philos. Trans. R. Soc. London*, *A315*, 509–562.

Elfouhaily, T., B. Chapron, and K. Katsaros (1997), A unified directional spectrum for long and short wind-driven waves, *J. Geophys. Res.*, *102*, 15,781–15,796.

Forristall, G. Z. (1981), Measurements of a saturated range in ocean wave spectra, *J. Geophys. Res.*, *86*, 8075–8084.

Frasier, S. J., Y. Liu, and R. E. McIntosh (1998), Space-Time properties of radar sea spikes and their relation to wind and wave conditions, *J. Geophys. Res.*, *103*, 18,745–18,757.

Hanson, J. L., and O. M. Phillips (2001), Automated analysis of ocean surface directional wave spectra, *J. Atmos. Ocean. Technol.*, *18*, 277–293.

Hanson, K. A., T. Hara, E. J. Bock, and A. B. Karachintsev (1997), Estimation of directional surface wave spectra from a towed research catamaran, *J. Atmos. Ocean. Technol.*, *14*, 1467–1482.

Hasselmann, K., et al. (1973), Measurements of wind-wave growth and swell decay during the Joint North Sea Wave Project (JONSWAP), *Dtsch. Hydrogr. Z.*, suppl. A, *8(12)*, 95pp.

Hauser, D., G. Caudal, S. Guimbard, and A. A. Mouche (2008), A study of the slope probability density function of the ocean waves from radar observations, *J. Geophys. Res.*, *113*, C02006, doi:10.1029/2007JC004264.

Hughes, B. A. (1976), The effect of internal waves on surface wind waves. 2: Theoretical analysis, *J. Geophys. Res.*, *83*, 455–465.

Hwang, P. A. (1997), A study of the wavenumber spectra of short water waves in the ocean. part 2: Spectral model and mean square slope, *J. Atmos. Ocean. Technol.*, *14*, 1174–1186.

Hwang, P. A. (2005), Wave number spectrum and mean-square slope of intermediate-scale ocean surface waves, *J. Geophys. Res.*, *110*, C10029, doi:10.1029/2005JC003002.

Hwang, P. A. (2006), Doppler frequency shift in ocean wave measurements: Frequency downshift of a wavenumber component by advection of background wave orbital velocity, *J. Geophys. Res.*, *111*, C06033, doi:10.1029/2005JC003072.

Hwang, P. A. (2007), Spectral signature of wave breaking in surface wave components of intermediate length scale, *J. Mar. Syst.*, *66*, 28–37.

Hwang, P. A. (2008), Comment on ''A study of the slope probability density function of the ocean waves from radar observations, by D. Hauser, G. Caudal, S. Guimbard, and A. A. Mouche,'' *J. Geophys. Res.*, doi:10.1029/2008JC005005, in press.

Hwang, P. A., and O. H. Shemdin (1988), The dependence of sea surface slope on atmospheric stability and swell conditions, *J. Geophys. Res.*, *93*, 13,903–13,912.

Hwang, P. A., and D. W. Wang (2001), Directional distributions and mean square slopes in the equilibrium and saturation ranges of the wave spectrum, *J. Phys. Oceanogr.*, *31*, 1346–1360.

Hwang, P. A., and D. W. Wang (2004a), An empirical investigation of source term balance of small scale surface waves, *Geophys. Res. Lett.*, *31*, L15301, doi:10.1029/2004GL020080.

Hwang, P. A., and D. W. Wang (2004b), Field measurements of duration limited growth of wind-generated ocean surface waves at young stage of development, *J. Phys. Oceanogr.*, *34*, 2316–2326, (Correction, *J. Phys. Oceanogr.*, *35*, 268–270, 2005).

Hwang, P. A., D. W. Wang, E. J. Walsh, W. B. Krabill, and R. N. Swift (2000), Airborne measurements of the directional wavenumber spectra of ocean surface waves. part 1: Spectral slope and dimensionless spectral coefficient, *J. Phys. Oceanogr.*, *30*, 2753–2767.

Hwang, P. A., M. A. Sletten, and J. V. Toporkov (2008a), Analysis of radar sea return for breaking wave investigation, *J. Geophys. Res.*, *113*, C02003, doi:10.1029/2007JC004319.

Hwang, P. A., M. A. Sletten, and J. V. Toporkov (2008b), Breaking wave contribution to low grazing angle radar backscatter from the ocean surface, *J. Geophys. Res.*, *113*, C09017, doi:10.1029/2008JC004752.

Jackson, F. C., W. T. Walton, D. E. Hines, B. A. Walter, and C. Y. Peng (1992), Sea surface mean-square slope from $K_u$-band backscatter data, *J. Geophys. Res.*, *97*, 11,411–11,427.

Jones, W. L., L. C. Schroeder, and K. L. Mitchell (1977), Aircraft measurements of the microwave scattering signature of the ocean, *IEEE J. Oceanic Eng.*, *2*, 52–61.

Liu, W. T., K. B. Katsaros, and J. A. Businger (1979), Bulk parameterization of air-sea exchanges of heat and water-vapor including the molecular constraints at the interface, *J. Atmos. Sci.*, *36*, 1722–1735.

Masuko, H., K. Okomoto, M. Shimada, and S. Niwa (1986), Measurement of microwave backscattering signatures of the ocean surface using $X$-band and $K_a$-band airborne scatterometers, *J. Geophys. Res.*, *91*, 13,065–13,083.

Mouche, A. A., D. Hauser, J. Daloze, and C. Guerin (2005), Dual-polarization measurements at C-band over the ocean: Results from airborne radar observations and comparison with ENVISAT ASAR data, *IEEE Trans. Geosci. Remote Sens.*, *43*, 753–769.

Phillips, O. M. (1977), *The Dynamics of the Upper Ocean*, 2nd ed., 336 pp., Cambridge Univ. Press, Cambridge, U.K.

Phillips, O. M. (1984), On the response of short ocean wave components at a fixed wavenumber to ocean current variations, *J. Phys. Oceanogr.*, *14*, 1425–1433.

Phillips, O. M. (1985), Spectral and statistical properties of the equilibrium range in wind-generated gravity waves, *J. Fluid Mech.*, *156*, 505–531.

Phillips, O. M. (1988), Radar return from the sea surface—Bragg scattering and breaking waves, *J. Phys. Oceanogr.*, *18*, 1065–1074.

Pierson, W. J., and L. Moskowitz (1964), A proposed spectral form for full, developed wind seas based on the similarity theory of S. A. Kitaigorodskii, *J. Geophys. Res.*, *69*, 5181–5190.

Plant, W. J. (1982), A relationship between wind stress and wave slope, *J. Geophys. Res.*, *87*, 1961–1967.

Plant, W. J. (2002), A stochastic, multiscale model of microwave backscatter from the ocean, *J. Geophys. Res.*, *107*(C9), 3120, doi:10.1029/2001JC000909.

Plant, W. J., and J. W. Wright (1977), Growth and equilibrium of short gravity waves in a wind-wave tank, *J. Fluid Mech.*, *82*, 767–793.

Tang, S., and O. H. Shemdin (1983), Measurement of high frequency waves using a wave follower, *J. Geophys. Res.*, *88*, 9832–9840.

Toba, Y. (1973), Local balance in the air-sea boundary processes. III: On the spectrum of wind waves, *J. Phys. Oceanogr.*, *3*, 579–593.

Vandemark, D., B. Chapron, J. Sun, G. H. Crescenti, and H. C. Graber (2004), Ocean wave slope observations using radar backscatter and laser altimeters, *J. Phys. Oceanogr.*, *34*, 2825–2842.

Walsh, E. J., D. C. Vandemark, C. A. Friehe, S. P. Burns, D. Khelif, R. N. Swift, and J. F. Scott (1998), Measuring sea surface mean square slope with a 36-GHz scanning radar altimeter, *J. Geophys. Res.*, *103*, 12,587–12,601.

Weissman, D. E., K. L. Davidson, R. A. Brown, C. A. Frieche, and F. Li (1994), Relationship between the microwave radar cross section and both wind speed and stress: Model function studies using Frontal Air-Sea Interaction Experiment data, *J. Geophys. Res.*, *99*, 10,087–10,108.

Wentz, F. J. (1977), A two scale scattering model with application to the JONSWAP '75 aircraft microwave scatterometer experiment, *NASA Contract Rep. 2919*, 122 p.

West, J. C., P. A. Hwang, R. K. Moore, J. C. Holtzman, and O. H. Shemdin (1990), The modulation of a radar signal from the ocean surface due to slope and hydrodynamic effects, *J. Geophys. Res.*, *95*, 16,291–16,297.

Wright, J. W. (1966), Backscattering from capillary waves with application to sea clutter, *IEEE Trans. Antennas Propag.*, *14*, 749–754.

Wright, J. W. (1968), A new model for sea clutter, *IEEE Trans. Antennas Propag.*, *16*, 217–223.

Young, I. R. (1995), The determination of confidence limits associated with estimates of the spectral peak frequency, *Ocean Eng.*, *22*, 669–686.

---

P. A. Hwang, Remote Sensing Division, Naval Research Laboratory, Code 7264, Building 2, Room 244E, 4555 Overlook Avenue SW, Washington, DC 20375, USA. (paul.hwang@nrl.navy.mil)